

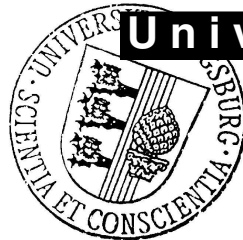
## On the return mapping algorithms in structural optimization of biomorphic ceramics

Ronald H. W. Hoppe, Svetozara I. Petrova

### Angaben zur Veröffentlichung / Publication details:

Hoppe, Ronald H. W., and Svetozara I. Petrova. 2007. "On the return mapping algorithms in structural optimization of biomorphic ceramics." Augsburg: Universität Augsburg.





**Universität Augsburg**

Institut für  
Mathematik

---

---

Ronald H.W. Hoppe, Svetozara I. Petrova

**On the Return Mapping Algorithms in Structural Optimization of  
Biomorphic Ceramics**

---

Preprint Nr. 019/2007 — 26. Juni 2007

Institut für Mathematik, Universitätsstraße, D-86 135 Augsburg

<http://www.math.uni-augsburg.de/>

---

**Impressum:**

*Herausgeber:*

Institut für Mathematik

Universität Augsburg

86135 Augsburg

<http://www.math.uni-augsburg.de/forschung/preprint/>

*ViSdP:*

Ronald H.W. Hoppe

Institut für Mathematik

Universität Augsburg

86135 Augsburg

*Preprint:* Sämtliche Rechte verbleiben den Autoren © 2007

# On the Return Mapping Algorithms in Structural Optimization of Biomorphic Ceramics

Ronald H.W. Hoppe and Svetozara I. Petrova \*

*Institute of Mathematics, University of Augsburg  
University Str. 14, D-86159 Augsburg, Germany  
{hoppe,petrova}@math.uni-augsburg.de*

## Abstract

The paper deals with structural optimization of biomorphic microcellular ceramics invoking an elasto–plasticity with the von Mises yield criterion in the macroscopic model. The return mapping algorithms introduced by Simo and Ortiz in 1985 are applied for the numerical solution of the problem. The latter methods are computationally effective, robust and stable, and have recently become the most popular means of numerically solving elasto–plastic equations. Based on the operator splitting methodology, the return mapping algorithm can be defined by first solving the elastic equations to obtain an elastic predictor and then taken as an initial condition for the plastic equations by using a projection of the trial elastic stress onto the constraint set of admissible stresses. Finite element discretized von Mises plasticity with isotropic strain hardening is included in the state equation considered as an equality constraint in the structural optimization problem.

**Keywords:** biomorphic ceramics, structural optimization, homogenization, elasto–plasticity, return mapping algorithms.

## 1 Introduction

Structural optimization of biomorphic cellular ceramics with specific microstructures is considered. The new composite materials are designed and produced by biotemplating processing using a naturally grown wood which is known to be highly porous and to possess excellent mechanical properties. High temperature pyrolysis of the wooden specimen followed by an infiltration of liquid– or gaseous–phase metals such as silicon (Si) or titanium (Ti) come up to silicon carbide (SiC)– or titanium carbide (TiC)–ceramics of high porosity. The biomimetic processing scheme for production of SiC–ceramics from wood is explained in [12]. The new ceramic composites can be used as filters in chemical processing, as implant material in biomedical applications or as high performance brakes of vehicles in car industry.

The optimization of the macroscopic behavior of microstructured materials using microscopic quantities as design variables is a well established discipline in materials science (cf., [1, 6, 11]). Homogenization techniques are applied to come up with computationally feasible macromodels. The microstructural geometrical details of the microcells such as the lengths and widths of the different layers forming the cell walls are considered as design parameters which have a significant impact on the macroscopic mechanical behavior of the final ceramics. Moreover, they can be tuned very precisely during the processing procedures. Therefore, the idea is to determine these details in order to achieve an optimal operational behavior with respect to selected mechanical merit functionals such as maximum rigidity (minimum compliance) under prespecified load conditions.

Recently, we have developed algorithmic tools for the computation of the homogenized model (homogenized elasticity tensor) and its dependence on the design variables as well as efficient and reliable structural optimization routines based on an "all-at-once" approach that is superior to traditional techniques (see, [8, 9, 10]). This includes a mesh adaptivity for the numerical solution of the elasticity problems defined in a 3–dimensional microcell and appropriate iterative schemes for the discretized state equation in the homogenized macromodel.

In this paper, we formulate the problem for structural optimization of the composite ceramic materials invoking an elasto–plasticity on the macroscopic model by using the von Mises yield criterion with isotropic strain

---

\*Permanent address: Institute for Parallel Processing, Bulgarian Academy of Sciences, Acad. G. Bontchev Str., Block 25A, 1113 Sofia, Bulgaria

hardening. An incremental finite element algorithm is presented for the numerical solution of the elasto–plastic problem. Return mapping procedures, first developed in [15], based on the concept of an elastic stress predictor mapped onto a suitably updated yield surface (plastic return corrector) are applied for the stress computation during the time increments. Note that the latter methods hold even for elasto–plastic materials with non–associated plasticity, general yield conditions, arbitrary flow and hardening rules, and variable tangent elastic moduli. In the last decade, they became rather popular tools to provide efficient and accurate computations for constitutive modeling (see, e.g., [3, 4, 14, 17]).

The following standard notations are used throughout this paper. Bold–face symbols indicate variables of tensorial character. By the convention of a summation on repeated indices, dots are used for a scalar product of vectors, e.g.  $\mathbf{u} \cdot \mathbf{v} = u_i v_i$  and colons ( $:$ ) are used for a scalar product of tensors, e.g.  $(\mathbf{E} : \mathbf{e})_{ij} = E_{ijkl} e_{kl}$ ,  $(\mathbf{A} : \mathbf{B}) = A_{ij} B_{ij}$ . The norm of a second–order tensor is denoted by  $\|\mathbf{S}\| = (\mathbf{S} : \mathbf{S})^{1/2} = (S_{ij} S_{ij})^{1/2}$ . The symbol  $\otimes$  indicates the tensor product of vectors and tensors defined by  $(\mathbf{u} \otimes \mathbf{v})_{ij} = u_i v_j$  and  $(\mathbf{A} \otimes \mathbf{B})_{ijkl} = A_{ij} B_{kl}$ .

## 2 Elasto–plasticity

Let us consider an elasto–plastic material body occupying a bounded Lipschitz domain  $\Omega \subset \mathcal{R}^3$ . For describing the development of plastic strains, we introduce a load/time (continuation) parameter  $t$ ,  $0 \leq t \leq T$  and find the deformations of the body following the history of loading. The dot below denotes the derivative with respect to the parameter  $t$ .

Given a displacement field  $\mathbf{u} = \mathbf{u}(\mathbf{x}, t) \in [H^1(\Omega)]^3$ , the total small strain reads

$$\mathbf{e} = (\nabla \mathbf{u} + (\nabla \mathbf{u})^T)/2, \quad (\text{i.e., } e(\mathbf{u})_{ij} = (u_{i,j} + u_{j,i})/2; \quad 1 \leq i, j \leq 3). \quad (1)$$

The following governing equations describe the elasto–plastic behavior of the material

$$\mathbf{e} = \mathbf{e}^e + \mathbf{e}^p \quad (2)$$

$$\dot{\mathbf{e}} = \dot{\mathbf{e}}^e + \dot{\mathbf{e}}^p \quad (3)$$

$$\boldsymbol{\sigma} = \mathbf{E} : \mathbf{e}^e \quad (4)$$

$$\Phi(\boldsymbol{\sigma}, \boldsymbol{\xi}) = 0 \quad (5)$$

$$\dot{\mathbf{e}}^p = \gamma \frac{\partial G}{\partial \boldsymbol{\sigma}} \quad (6)$$

$$\dot{\boldsymbol{\xi}} = \gamma \mathbf{z}, \quad (7)$$

where the total strain  $\mathbf{e}$  is decomposed into an elastic and plastic strain tensors denoted by  $\mathbf{e}^e$  and  $\mathbf{e}^p$ , respectively,  $\boldsymbol{\sigma}$  is the Cauchy stress tensor,  $\mathbf{E}$  is the forth–order elasticity tensor,  $\Phi = \Phi(\boldsymbol{\sigma}, \boldsymbol{\xi}) \leq 0$  is the yield function,  $\boldsymbol{\xi} \in \mathcal{R}^k$ ,  $k \geq 1$ , is the vector of internal state variables,  $\gamma \geq 0$  is the plastic multiplier (also called the magnitude of the plastic strain rate),  $G$  is the flow potential, and  $\mathbf{z}$  is a vector related to the evolution of the internal state variables  $\boldsymbol{\xi}$ . Note that  $\boldsymbol{\xi}$  and  $\mathbf{z}$  are scalars in the case  $k = 1$ . We assume that the scalar–valued function  $G$  is differentiable everywhere and  $\partial G / \partial \boldsymbol{\sigma}$  is a second–order tensor produced by differentiation of  $G$  with respect to the tensorial argument  $\boldsymbol{\sigma}$ .

Linear isotropic and homogeneous elasticity is considered, so that Eq. (4) is referred to Hooke’s law which corresponds to a two–parameter model with nonzero material coefficients given as follows

$$E_{iiii} = \lambda + 2\mu, \quad E_{iijj} = \lambda, \quad E_{ijij} = E_{ijji} = 2\mu, \quad (8)$$

where  $1 \leq i, j \leq 3$ ,  $i \neq j$ , and  $\lambda, \mu$  are the Lamé moduli of the material. Very often in the literature the isotropic materials are also described by the Young modulus  $E$  and the Poisson ratio  $\nu$ .

Eq. (5) defines the yield surface and can be viewed as the onset of the inelastic behavior of the material. The yield function  $\Phi$  obeys the sign convention: elastic deformations correspond to negative values of  $\Phi$  (the interior of the yield surface) and forbidden deformations (on the exterior of the yield surface) are identified by positive values of  $\Phi$ . Hence, all admissible stresses are described by  $\Phi(\boldsymbol{\sigma}, \boldsymbol{\xi}) \leq 0$  and exactly one of the following relations holds

$$\begin{aligned} \gamma = 0 \wedge \Phi(\boldsymbol{\sigma}, \boldsymbol{\xi}) < 0, & \quad \text{elastic behavior} \\ \gamma > 0 \wedge \Phi(\boldsymbol{\sigma}, \boldsymbol{\xi}) = 0 \wedge \dot{\Phi}(\boldsymbol{\sigma}, \boldsymbol{\xi}) = 0, & \quad \text{plastic behavior} \end{aligned} \quad (9)$$

These relations are explicitly described by the Karush–Kuhn–Tucker (KKT) complementarity conditions which take place both for elastic and plastic deformations:

$$\gamma \geq 0, \quad \Phi(\boldsymbol{\sigma}, \boldsymbol{\xi}) \leq 0, \quad \gamma \Phi(\boldsymbol{\sigma}, \boldsymbol{\xi}) = 0. \quad (10)$$

The parameter  $\gamma \geq 0$  in (10) is determined by the consistency condition  $\dot{\Phi}(\boldsymbol{\sigma}, \boldsymbol{\xi}) = 0$ . Note that  $\gamma$  is nonzero only if  $\Phi = \dot{\Phi} = 0$ , see (9). For details we refer to [14].

The plastic flow rule is expressed by (6). In the case of associative plasticity (typically applied to porous solids) the flow function becomes  $G = \Phi$  and the associative flow rule of plastic deformation is given by

$$\dot{\boldsymbol{\epsilon}}^p = \gamma \frac{\partial \Phi}{\partial \boldsymbol{\sigma}}. \quad (11)$$

The constitutive relation (4) can be written in a rate form  $\dot{\boldsymbol{\sigma}} = \mathbf{E} : \dot{\boldsymbol{\epsilon}}^e$ . Using (3) and (11) the following expression holds

$$\dot{\boldsymbol{\sigma}} = \mathbf{E} : \left( \dot{\boldsymbol{\epsilon}} - \gamma \frac{\partial \Phi}{\partial \boldsymbol{\sigma}} \right). \quad (12)$$

Multiplying (12) by  $\frac{\partial \Phi}{\partial \boldsymbol{\sigma}}$  we get

$$\frac{\partial \Phi}{\partial \boldsymbol{\sigma}} : \dot{\boldsymbol{\sigma}} = \frac{\partial \Phi}{\partial \boldsymbol{\sigma}} : \mathbf{E} : \dot{\boldsymbol{\epsilon}} - \gamma \frac{\partial \Phi}{\partial \boldsymbol{\sigma}} : \mathbf{E} : \frac{\partial \Phi}{\partial \boldsymbol{\sigma}}. \quad (13)$$

To eliminate  $\gamma$  we take the rate form of Eq. (5) as follows

$$\dot{\Phi}(\boldsymbol{\sigma}, \boldsymbol{\xi}) = 0, \quad (14)$$

which using the chain rule reads

$$\frac{\partial \Phi}{\partial \boldsymbol{\sigma}} : \dot{\boldsymbol{\sigma}} + \frac{\partial \Phi}{\partial \boldsymbol{\xi}} \cdot \dot{\boldsymbol{\xi}} = 0. \quad (15)$$

Replacing (13) and (7) in (15) we get the following expression

$$\frac{\partial \Phi}{\partial \boldsymbol{\sigma}} : \mathbf{E} : \dot{\boldsymbol{\epsilon}} - \gamma \left( \frac{\partial \Phi}{\partial \boldsymbol{\sigma}} : \mathbf{E} : \frac{\partial \Phi}{\partial \boldsymbol{\sigma}} - \frac{\partial \Phi}{\partial \boldsymbol{\xi}} \cdot \mathbf{z} \right) = 0. \quad (16)$$

Thus, the plastic multiplier can be defined explicitly as

$$\gamma = \frac{\frac{\partial \Phi}{\partial \boldsymbol{\sigma}} : \mathbf{E} : \dot{\boldsymbol{\epsilon}}}{\frac{\partial \Phi}{\partial \boldsymbol{\sigma}} : \mathbf{E} : \frac{\partial \Phi}{\partial \boldsymbol{\sigma}} - \frac{\partial \Phi}{\partial \boldsymbol{\xi}} \cdot \mathbf{z}}. \quad (17)$$

Substituting  $\gamma$  in (12) we get

$$\dot{\boldsymbol{\sigma}} = \mathbf{E}^{ep} : \dot{\boldsymbol{\epsilon}}, \quad (18)$$

where the continuum tangent modulus  $\mathbf{E}^{ep}$  (also called the elasto–plastic tangent operator) is given by

$$\mathbf{E}^{ep} = \mathbf{E}^{ep}(\boldsymbol{\sigma}, \boldsymbol{\xi}, \dot{\boldsymbol{\epsilon}}) = \begin{cases} \mathbf{E} & \text{if } \Phi(\boldsymbol{\sigma}, \boldsymbol{\xi}) < 0, \\ \mathbf{E} - \frac{\mathbf{E} : \frac{\partial \Phi}{\partial \boldsymbol{\sigma}} \otimes \frac{\partial \Phi}{\partial \boldsymbol{\sigma}} : \mathbf{E}}{\frac{\partial \Phi}{\partial \boldsymbol{\sigma}} : \mathbf{E} : \frac{\partial \Phi}{\partial \boldsymbol{\sigma}} - \frac{\partial \Phi}{\partial \boldsymbol{\xi}} \cdot \mathbf{z}} & \text{if } \Phi(\boldsymbol{\sigma}, \boldsymbol{\xi}) = 0. \end{cases} \quad (19)$$

Using Eq. (17) one can rewrite (7) in the form

$$\dot{\boldsymbol{\xi}} = \mathbf{G}^{ep} : \dot{\boldsymbol{\epsilon}}, \quad (20)$$

where

$$\mathbf{G}^{ep} = \mathbf{G}^{ep}(\boldsymbol{\sigma}, \boldsymbol{\xi}, \dot{\boldsymbol{\epsilon}}) = \begin{cases} \mathbf{0} & \text{if } \Phi(\boldsymbol{\sigma}, \boldsymbol{\xi}) < 0, \\ \frac{\frac{\partial \Phi}{\partial \boldsymbol{\sigma}} : \mathbf{E} : \mathbf{z}}{\frac{\partial \Phi}{\partial \boldsymbol{\sigma}} : \mathbf{E} : \frac{\partial \Phi}{\partial \boldsymbol{\sigma}} - \frac{\partial \Phi}{\partial \boldsymbol{\xi}} \cdot \mathbf{z}} & \text{if } \Phi(\boldsymbol{\sigma}, \boldsymbol{\xi}) = 0. \end{cases} \quad (21)$$

The expressions (18) and (20) are called the incremental elasto–plastic constitutive relations derived under the assumption (14) during the plastic yielding.

We suppose now that the elasto–plastic body occupying the domain  $\Omega$  is fixed on the part  $\Gamma_D$  of its boundary  $\partial\Omega$ ,  $\Gamma_D \subset \partial\Omega$ , and loaded by the body force  $\mathbf{f}_b$  in  $\Omega$  and by the surface traction  $\mathbf{f}_s$  on the rest part of the boundary  $\Gamma_T$ ,  $\Gamma_T \subset \partial\Omega$ ,  $\Gamma_D \cup \Gamma_T = \partial\Omega$ . Taking into account the continuation of loading with respect to the

time parameter  $t \in [0, T] \subset \mathcal{R}$  one can formulate the problem of elasto–plasticity as the following initial value problem: Find

$$\mathbf{u} = \mathbf{u}(\mathbf{x}, t), \quad \boldsymbol{\sigma} = \boldsymbol{\sigma}(\mathbf{x}, t), \quad \boldsymbol{\xi} = \boldsymbol{\xi}(\mathbf{x}, t),$$

such that

$$\begin{aligned} \int_{\Omega} \dot{\boldsymbol{\sigma}} : \mathbf{e}(\mathbf{v}) \, dx &= (\dot{\mathbf{F}}, \mathbf{v}), \quad \forall \mathbf{v} \in \mathbf{V}, \quad t \in [0, T] \\ \dot{\boldsymbol{\sigma}} &= \mathbf{E}^{ep}(\boldsymbol{\sigma}, \boldsymbol{\xi}, \dot{\mathbf{e}}) : \dot{\mathbf{e}} \\ \dot{\boldsymbol{\xi}} &= \mathbf{G}^{ep}(\boldsymbol{\sigma}, \boldsymbol{\xi}, \dot{\mathbf{e}}) : \dot{\mathbf{e}} \\ \dot{\mathbf{e}} &= \mathbf{e}(\dot{\mathbf{u}}), \quad \dot{\mathbf{u}} \in \mathbf{V} \end{aligned} \tag{22}$$

with initial conditions

$$\mathbf{u} = \mathbf{u}(\mathbf{x}, 0) = \mathbf{0}, \quad \boldsymbol{\sigma} = \boldsymbol{\sigma}(\mathbf{x}, 0) = \mathbf{0}, \quad \boldsymbol{\xi} = \boldsymbol{\xi}(\mathbf{x}, 0) = \mathbf{0}, \quad \forall \mathbf{x} \in \Omega.$$

Here,  $\mathbf{u}$  refers to the 3-dimensional displacement vector,  $\mathbf{x}$  is the space variable in  $\Omega$ ,  $\mathbf{V}$  is the space of admissible displacements  $\mathbf{V} := \{\mathbf{v} \in [H^1(\Omega)]^3 \mid \mathbf{v} = \mathbf{0} \text{ on } \Gamma_D\}$  and  $\mathbf{F}$  is the function of all external forces with an inner product defined as follows

$$(\dot{\mathbf{F}}, \mathbf{v}) = \int_{\Omega} \dot{\mathbf{f}}_b \cdot \mathbf{v} \, dx + \int_{\Gamma_T} \dot{\mathbf{f}}_s \cdot \mathbf{v} \, ds.$$

Note that (22) represents the incremental equilibrium equation in a weak form, see, e.g., [4].

### 3 Incremental finite element elasto–plasticity

In this section, we present the discrete analog of the initial value problem (22) by using finite differences with respect to the time parameter  $t$  and finite elements with respect to the space variable  $\mathbf{x}$ . We introduce the following temporal mesh in the interval  $[0, T] \subset \mathcal{R}$

$$t^0 = 0, \quad t^{n+1} = t^n + \Delta t, \quad n = 0, \dots, N, \quad N = T/\Delta t - 1. \tag{23}$$

The domain  $\Omega$  is discretized by finite elements with a discretization parameter  $h$ . Using rates one can exploit the following incremental relation

$$\Delta \boldsymbol{\sigma}_h = \int_{t^n}^{t^{n+1}} \dot{\boldsymbol{\sigma}}_h \, dt, \quad t \in [t^n, t^{n+1}].$$

For a fixed time step  $t^n = n\Delta t$  we approximate the displacement vector  $\mathbf{u}(\mathbf{x}, t^n)$ , the stress tensor  $\boldsymbol{\sigma}(\mathbf{x}, t^n)$ , and the vector of internal variables  $\boldsymbol{\xi}(\mathbf{x}, t^n)$ , respectively by

$$\mathbf{u}_h^n(\mathbf{x}), \quad \boldsymbol{\sigma}_h^n(\mathbf{x}), \quad \boldsymbol{\xi}_h^n(\mathbf{x}),$$

where  $\mathbf{u}_h^n \in \mathbf{V}_h$ ,  $\mathbf{V}_h$  is the finite element subspace of  $\mathbf{V}$ ,  $\boldsymbol{\sigma}_h^n$  and  $\boldsymbol{\xi}_h^n$  belong to the corresponding discrete spaces of stresses and internal variables.

For given  $\mathbf{u}_h^n$ ,  $\boldsymbol{\sigma}_h^n$ ,  $\boldsymbol{\xi}_h^n$ , the increments  $\Delta \mathbf{u}_h$ ,  $\Delta \boldsymbol{\sigma}_h$ ,  $\Delta \boldsymbol{\xi}_h$  at the time step  $t^n$ ,  $n = 0, \dots, N$ , can be determined by using the following incremental finite element (FE) algorithm

S1. *Initial step:*  $\mathbf{u}_h^0 = \mathbf{0}$ ,  $\boldsymbol{\sigma}_h^0 = \mathbf{0}$ ,  $\boldsymbol{\xi}_h^0 = \mathbf{0}$

S2. *Load steps:* **for**  $n = 0, \dots, N$  **do**

- Given  $\mathbf{u}_h^n$ ,  $\boldsymbol{\sigma}_h^n$ ,  $\boldsymbol{\xi}_h^n$ ,
- Compute the increments  $\Delta \mathbf{u}_h$ ,  $\Delta \boldsymbol{\sigma}_h$ ,  $\Delta \boldsymbol{\xi}_h$ , such that

$$\int_{\Omega} \Delta \boldsymbol{\sigma}_h : \mathbf{e}(\mathbf{v}_h) \, dx = (\Delta \mathbf{F}, \mathbf{v}_h), \quad \forall \mathbf{v}_h \in \mathbf{V}_h, \tag{24}$$

$$\Delta \boldsymbol{\sigma}_h = \mathbf{E}^{ep}(\boldsymbol{\sigma}_h^n + \theta \Delta \boldsymbol{\sigma}_h, \boldsymbol{\xi}_h^n + \theta \Delta \boldsymbol{\xi}_h, \Delta \mathbf{e}_h) : \Delta \mathbf{e}_h, \tag{25}$$

$$\Delta \boldsymbol{\xi}_h = \mathbf{G}^{ep}(\boldsymbol{\sigma}_h^n + \theta \Delta \boldsymbol{\sigma}_h, \boldsymbol{\xi}_h^n + \theta \Delta \boldsymbol{\xi}_h, \Delta \mathbf{e}_h) : \Delta \mathbf{e}_h, \tag{26}$$

$$\Delta \mathbf{e}_h = \mathbf{e}(\Delta \mathbf{u}_h), \quad \Delta \mathbf{u}_h \in \mathbf{V}_h. \tag{27}$$

- Put  $\mathbf{u}_h^{n+1} = \mathbf{u}_h^n + \Delta \mathbf{u}_h$ ,  $\boldsymbol{\sigma}_h^{n+1} = \boldsymbol{\sigma}_h^n + \Delta \boldsymbol{\sigma}_h$ ,  $\boldsymbol{\xi}_h^{n+1} = \boldsymbol{\xi}_h^n + \Delta \boldsymbol{\xi}_h$ .

S3. **End**

The right hand side in Eq. (24) is computed as follows

$$(\Delta \mathbf{F}, \mathbf{v}_h) = \int_{\Omega} \Delta \mathbf{f}_b \cdot \mathbf{v}_h dx + \int_{\Gamma_T} \Delta \mathbf{f}_s \cdot \mathbf{v}_h ds, \quad (28)$$

where

$$\Delta \mathbf{f}_b(\mathbf{x}) = \mathbf{f}_b(\mathbf{x}, t^{n+1}) - \mathbf{f}_b(\mathbf{x}, t^n), \quad \Delta \mathbf{f}_s(\mathbf{x}) = \mathbf{f}_s(\mathbf{x}, t^{n+1}) - \mathbf{f}_s(\mathbf{x}, t^n).$$

Note that  $\theta \in [0, 1]$  is a parameter. The choice of  $\theta = 0$  resembles the forward (explicit) Euler method,  $\theta = 1/2$  indicates the midpoint rule, and  $\theta = 1$  corresponds to the backward (implicit) Euler scheme (see, e.g., [14]). Hence, the algorithm above refers to as the explicit ( $\theta = 0$ ) and implicit ( $\theta = 1$ ) incremental FE method, respectively. The question of consistency, numerical stability and accuracy of the forward and backward Euler integration algorithms is discussed in [17]. The essential difficulty in the incremental finite element method is the computation of  $\mathbf{E}^{ep}$  and  $\mathbf{G}^{ep}$  which depend at a fixed time step  $t^n$  on the stress and the vector of internal variables. Note that in the case  $\theta = 0$  the values of  $\partial \Phi / \partial \boldsymbol{\sigma}$ ,  $\partial \Phi / \partial \boldsymbol{\xi}$ , and  $\mathbf{z}$  in (19) and (21) are computed at the beginning of the time increment and hence, at each time step they are known in advance.

Iterative solution schemes based on Newton's method to compute the increments  $\Delta \mathbf{u}_h$ ,  $\Delta \boldsymbol{\sigma}_h$ ,  $\Delta \boldsymbol{\xi}_h$  are widely used in the literature (cf., e.g., [4, 5, 16, 17]). Typically, for each  $n$ ,  $0 \leq n \leq N$ , in step [S2] of the incremental FE algorithm, one has to solve a nonlinear system to find  $\Delta \mathbf{u}_h$ . The solution of this nonlinear system requires applications of Newton-like algorithms in which a sequence of linear problems has to be solved (see [5] for details). The use of the so-called consistent tangent moduli within the finite element approach was first proposed in [16] where a consistently linearization of the nonlinear problem based on the closest-point return mapping algorithms is applied in order to preserve the quadratic rate of asymptotic convergence of Newton's method. The analysis in this work is done for rate-independent plasticity with arbitrary rules of isotropic and kinematic hardening. In this particular case, the closest-point projection leads to the so-called radial return algorithms where explicit expressions for the tangent moduli consistent with the integration algorithm can be derived (see [16] for details). When the return is non-radial, an essential drawback in practical computations is the necessity of matrix inversions to solve the return equations (see, [3, 14, 17]).

## 4 Return mapping algorithm

We apply the return mapping algorithms based on the concept of operators splitting for the numerical solution of the elasto-plastic problem within the incremental FE method described in Section 3. For pioneering works in this area we refer the reader to [15, 16]. Details and generalizations of these algorithms can be found in [14].

For convenience of the presentation, we omit the discretization space parameter  $h$  and use the following notations for the increments:  $\Delta \boldsymbol{\sigma} = \Delta \boldsymbol{\sigma}_h(\mathbf{x})$ ,  $\Delta \mathbf{e} = \Delta \mathbf{e}_h(\mathbf{x})$ ,  $\Delta \boldsymbol{\xi} = \Delta \boldsymbol{\xi}_h(\mathbf{x})$ , at a fixed load step  $t^n$ ,  $0 \leq n \leq N$ . For given initial values of  $\boldsymbol{\sigma}^n$  and  $\boldsymbol{\xi}^n$  the problem is to find the evolution of these values over the interval  $[t^n, t^{n+1}]$ .

The basic idea of the return algorithms is the following: A trial stress  $\boldsymbol{\sigma}^{trial}$  is involved by taking the entire step to be elastic (elastic predictor). The computed trial stress is categorized to be elastic or plastic by checking the sign of the yield function  $\Phi$ . If the predicted trial stress happens to fall outside the yield surface ( $\Phi > 0$ ) then our assumption of elasticity has been wrong and the updated stress  $\boldsymbol{\sigma}^{n+1}$  is obtained by the orthogonal projection (closest-point projection) of the trial stress onto the updated yield surface (plastic corrector). The return path is visualized on Fig. 1 in case of perfect plasticity (i.e.,  $\boldsymbol{\xi} \equiv 0$ ).

Using (2), (4), and (11) the final updated stress  $\boldsymbol{\sigma}^{n+1}$  can be successively expressed as follows:

$$\boldsymbol{\sigma}^{n+1} = \mathbf{E}: \left( \mathbf{e}^{n+1} - (\mathbf{e}^p)^{n+1} \right) \quad (29)$$

$$= \mathbf{E}: (\mathbf{e}^{n+1} - (\mathbf{e}^p)^n) - \mathbf{E}: \left( (\mathbf{e}^p)^{n+1} - (\mathbf{e}^p)^n \right) \quad (30)$$

$$= \mathbf{E}: \mathbf{e}^{n+1} - \mathbf{E}: (\mathbf{e}^n - (\mathbf{e}^e)^n) - \mathbf{E}: \Delta \mathbf{e}^p \quad (31)$$

$$= \mathbf{E}: (\mathbf{e}^e)^n + \mathbf{E}: (\mathbf{e}^{n+1} - \mathbf{e}^n) - \mathbf{E}: \Delta \mathbf{e}^p \quad (32)$$

$$= \boldsymbol{\sigma}^n + \mathbf{E}: \Delta \mathbf{e} - \Delta \gamma \mathbf{E}: \frac{\partial \Phi}{\partial \boldsymbol{\sigma}} \quad (33)$$

$$= \boldsymbol{\sigma}^{trial} - \Delta \gamma \mathbf{E}: \frac{\partial \Phi}{\partial \boldsymbol{\sigma}}, \quad (34)$$

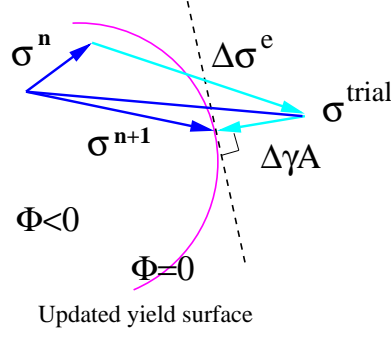


Figure 1: Mapping the trial stress back to the yield surface (perfect plasticity)

where  $\Delta\gamma = \gamma^{n+1}\Delta t \geq 0$ . This choice corresponds to the backward Euler scheme and leads to the classical return mapping algorithms.

For a given total strain increment  $\Delta e$  the following two steps are applied in the return mapping process:

1. *Elastic predictor*: Compute the trial stress  $\sigma^{trial}$  assuming only elastic behavior

$$\sigma^{trial} = \sigma^n + \Delta\sigma^e \quad \text{with} \quad \Delta\sigma^e = \mathbf{E} : \Delta e. \quad (35)$$

2. *Plastic corrector*: Compute the updated stress and the internal variables

$$\sigma^{n+1} = \sigma^{trial} - \Delta\gamma \mathbf{A}, \quad \mathbf{A} = \mathbf{E} : \frac{\partial\Phi}{\partial\sigma}, \quad (36)$$

$$\xi^{n+1} = \xi^n + \Delta\xi, \quad \Delta\xi = \Delta\gamma z, \quad (37)$$

where  $\partial\Phi/\partial\sigma$  and  $z$  are computed at the end of the time increment. Note that  $\mathbf{A}$  is a second-order tensor called the projection direction (see Fig. 1). One can see from Eq. (33) that the updated stress  $\sigma^{n+1} = \sigma^n + \Delta\sigma$  can be found with a stress increment  $\Delta\sigma$  determined according to the sign of the yield function  $\Phi$ , namely:

$$\Delta\sigma = \begin{cases} \mathbf{E} : \Delta e & \text{if } \Phi(\sigma^{trial}, \xi^n) \leq 0, \\ \mathbf{E} : \Delta e - \Delta\gamma \mathbf{E} : \frac{\partial\Phi}{\partial\sigma} & \text{if } \Phi(\sigma^{trial}, \xi^n) > 0. \end{cases} \quad (38)$$

Therefore, we simply set  $\sigma^{n+1} = \sigma^{trial}$  in the case  $\Phi(\sigma^{trial}, \xi^n) \leq 0$ . Otherwise, one computes the plastic return of the trial stress onto the yield surface according to Eq. (36). The discrete plastic multiplier  $\Delta\gamma$  is updated satisfying the yield consistency condition (14) at the end of the time increment:

$$\dot{\Phi}(\sigma^{n+1}, \xi^{n+1}) = 0. \quad (39)$$

In general, the return mapping of the trial stress back to the yield surface is nonlinear and it should be performed iteratively according to the Newton method with consistently linearised stress-strain relations. Thus, the proper choice of tangent moduli consistent with the proposed return mapping procedure has a strong influence on the convergence rate of the iterative schemes and the diminishing of the computational work. Consistent tangent moduli based on an exact linearization of the nonlinear problem have been originally proposed in [16] and recently developed, for instance, in [3, 14].

In practical computations we emphasize on the classical von Mises constitutive relations which can be involved in various modifications (perfect plasticity or isotropic/kinematic hardening). For details we follow [14] and the references therein. We use as a model example the von Mises plasticity with isotropic strain hardening which fits to the porous composite ceramic materials when consider mechanical damages due to the growth and nucleation of voids. This model is given by

$$\Phi(\sigma, \xi) = \sqrt{\frac{3}{2}} \|\text{dev}(\sigma)\| - \mathcal{H}(\xi) \quad (40)$$

$$\xi = \sqrt{\frac{2}{3}} \|e^p\|, \quad (41)$$

where  $\text{dev}(\boldsymbol{\sigma}) = \boldsymbol{\sigma} - \frac{1}{3}\text{tr}(\boldsymbol{\sigma})\mathbf{1}$  denotes the deviatoric stress tensor and  $\mathbf{1}$  is the second-order symmetric unit tensor.  $\mathcal{H}$  is a given function derived experimentally. It is assumed to be twice differentiable with the following relations

$$\mathcal{H}(\boldsymbol{\xi}) \geq \mathcal{H}_0 > 0, \quad \mathcal{H}'(\boldsymbol{\xi}) \geq \mathcal{H}_1 > 0, \quad |\mathcal{H}''(\boldsymbol{\xi})| \leq \mathcal{H}_2, \quad \forall \boldsymbol{\xi} \geq 0. \quad (42)$$

The values of  $\partial\Phi/\partial\boldsymbol{\sigma}$  and  $\partial\Phi/\partial\boldsymbol{\xi}$  which take part in (19) and (21) can be easily computed

$$\frac{\partial\Phi}{\partial\boldsymbol{\sigma}} = \sqrt{\frac{3}{2}} \frac{\text{dev}(\boldsymbol{\sigma})}{\|\text{dev}(\boldsymbol{\sigma})\|}, \quad \frac{\partial\Phi}{\partial\boldsymbol{\xi}} = -\mathcal{H}'. \quad (43)$$

The function  $\mathcal{H}'(\boldsymbol{\xi})$  is called the isotropic hardening modulus. By (7), (11), and (41) we find  $\mathbf{z}$  as follows

$$\dot{\boldsymbol{\xi}} = \sqrt{\frac{2}{3}}\|\dot{\boldsymbol{e}}^p\| = \sqrt{\frac{2}{3}}\gamma \left\| \frac{\partial\Phi}{\partial\boldsymbol{\sigma}} \right\| = \gamma \mathbf{z}, \quad \implies \mathbf{z} = \sqrt{\frac{2}{3}} \left\| \frac{\partial\Phi}{\partial\boldsymbol{\sigma}} \right\| = 1. \quad (44)$$

Note that in this particular case the closest-point projection can be explicitly defined where no operator inversion is required. Here, one faces with the so-called radial return mapping algorithms whose efficiency is well established [14, 16].

## 5 Structural optimization

The problem of structural optimization of microcellular biomorphic TiC-ceramics is discussed in this section. As noted in Section 1, the materials under consideration are microstructural and hence, their macroscopic mechanical behavior strongly depends on microscopic geometrical quantities such as the size of the voids and the lengths and widths of the different layers forming the cell walls [7]. While the size of the voids is determined by the growth of the wood itself (early/late wood), the other quantities can be influenced by tuning the parameters within the biotemplating process. Denote these geometrical quantities by  $\boldsymbol{\alpha} = (\alpha_1, \dots, \alpha_m)^T$ , further referred to as design parameters.

We consider a 3-dimensional stationary microstructure with a geometrically simple tracheidal periodicity cell  $Y = [0, 1]^3$  (see Fig. 2) consisting of an outer layer of carbon ( $C$ ), interior layer of TiC, and a void channel (no material). In this particular case the number of layers is  $m = 2$ . We assume that our material workpiece occupies the bounded domain  $\Omega \subset \mathcal{R}^3$  with periodically distributed constituents ( $C$ , TiC, and Void).

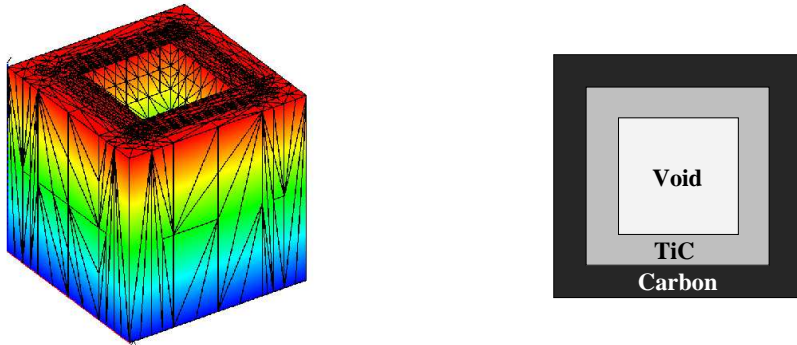


Figure 2: a) Periodicity cell  $Y = [0, 1]^3$ , b) Cross section of  $Y = \text{Void} \cup \text{TiC} \cup C$

The optimal structural design of the biomorphic microcellular ceramics can be performed by solving the following structural optimization problem

$$J(\mathbf{u}, \boldsymbol{\alpha}) = \inf_{\mathbf{v}, \boldsymbol{\beta}} J(\mathbf{v}, \boldsymbol{\beta}), \quad (45)$$

subject to the equality constraints

$$\text{Eq. (22)} \quad \text{with} \quad \boldsymbol{\sigma} = \boldsymbol{\sigma}(x, t, \boldsymbol{\alpha}) \quad (46)$$

$$\sum_{i=1}^m \alpha_i := C \quad (47)$$

and the inequality constraints

$$\alpha_i^{(min)} \leq \alpha_i \leq \alpha_i^{(max)} \quad , \quad 1 \leq i \leq m \quad , \quad (48)$$

where the equality constraint (47) with a given constant  $C$  and the bounds  $\alpha_i^{(min)}, \alpha_i^{(max)}$ ,  $1 \leq i \leq m$ , in (48) stand for constraints motivated by both the microstructural geometry of the carbon preform and the biotemplating process. The von Mises plasticity with isotropic strain hardening is included in the state equation (46). The objective functional  $J$  depends on the mode of loading (cf., e.g., [2, 7, 13] for a variety of mechanical merit criteria). Note that the resolution of the microstructures is cost prohibitive with respect to computational work. Thus, the main idea is to derive a homogenized macromodel featuring the dependence on the microstructural design variables and to apply the optimization process to the homogenized model. More precisely, the state equation (22) is considered as an equality constraint taking into account the dependence of the stress  $\boldsymbol{\sigma}$  on the design parameters  $\boldsymbol{\alpha}$ , i.e., everywhere in the expressions for  $\mathbf{E}^{ep}$  and  $\mathbf{G}^{ep}$  the elasticity tensor  $\mathbf{E}$  is now replaced by the homogenized (forth-order) elasticity tensor  $\mathbf{E}^H = \mathbf{E}^H(\boldsymbol{\alpha})$ . Following [11], the homogenization approach based on the standard double scale asymptotic expansion of the unknown displacement vector is applied to find the homogenized coefficients as follows

$$E_{ijkl}^H = \frac{1}{|Y|} \int_Y (E_{ijkl}(y) - E_{ijpq}(y) \frac{\partial \zeta_p^{kl}}{\partial y_q}) dy \quad . \quad (49)$$

The third-order tensor  $\boldsymbol{\zeta} = (\zeta_p^{kl})$ ,  $k, l, p = 1, 2, 3$ , with periodic components (i.e., equal values on opposite sides of  $Y$ )  $\zeta_p^{kl} \in H^1(Y)$  has to be computed by solving the elasticity problems

$$\int_Y \left( E_{ijpq}(y) \frac{\partial \zeta_p^{kl}}{\partial y_q} \right) \frac{\partial \phi_i}{\partial y_j} dy = \int_Y E_{ijkl}(y) \frac{\partial \phi_i}{\partial y_j} dy \quad (50)$$

for an arbitrary  $Y$ -periodic variational function  $\phi \in [H^1(Y)]^3$ . The computation of the homogenized elasticity tensor can be done analytically for some specific geometries as, for instance, layered materials or checkerboard structures (cf., e.g., [11]). For more complicated microstructures, the computation of the homogenized coefficients  $E_{ijkl}^H$  has to be done numerically (see [8] for details). We solve Eq. (50) by finite element discretizations using continuous, piecewise linear basis functions on tetrahedral shape regular meshes. Adaptive grid refinement algorithms based on a posteriori error estimators as well as efficient solvers for the 3-dimensional model are developed in [10]. We find the dependence of the homogenized tensor  $\mathbf{E}^H = \mathbf{E}^H(\boldsymbol{\alpha})$  on the design parameters  $\boldsymbol{\alpha}$  by means of multivariate interpolation. The Young modulus  $E$  (in GPa) and the Poisson ratio  $\nu$  of our two materials are, respectively,  $E = 10$ ,  $\nu = 0.22$  for carbon and  $E = 439$ ,  $\nu = 0.187$  for TiC. Some numerical experiments from the computation of the homogenized coefficients with respect to the consecutive number of adaptive level are presented in Table 1.

level	$E_{1111}^H$	$E_{2222}^H$	$E_{3333}^H$	$E_{1212}^H$	$E_{2323}^H$	$E_{1313}^H$	$E_{1111}^H$	$E_{2222}^H$	$E_{3333}^H$	$E_{1212}^H$	$E_{2323}^H$	$E_{1313}^H$
1	179.7	192.4	224.2	67.4	75.5	64.0	168.6	174.2	180.2	63.6	66.8	62.3
2	197.4	227.0	238.1	80.7	99.1	69.8	178.6	191.1	194.7	75.2	79.7	71.4
3	177.6	188.7	226.9	60.9	73.1	63.1	167.2	179.1	192.3	63.9	70.7	68.8
4	190.2	184.3	235.7	69.7	72.0	81.5	172.7	157.3	188.9	51.4	60.2	70.8
5	184.5	180.6	236.1	46.3	57.4	86.6	154.0	153.1	192.0	48.1	63.1	64.0
6	171.5	156.0	228.1	31.0	58.3	56.9	123.5	125.4	190.0	37.9	51.1	51.0
7	177.6	151.5	234.1	29.1	59.1	76.8	104.7	109.8	187.9	34.4	46.8	50.3
8	170.9	152.7	232.5	26.5	59.3	64.4	99.6	99.7	187.7	30.4	48.1	48.4
9	161.6	148.9	230.0	36.6	57.8	59.2	88.1	90.3	186.3	26.5	45.0	46.2
10	146.9	145.7	230.3	28.5	55.2	57.3	84.0	84.3	185.8	26.6	43.8	43.5

Table 1: Homogenized coefficients for early wood, density 19%,  $\alpha_1 = \alpha_2 = 0.025$  and for late wood, density 84%,  $\alpha_1 = \alpha_2 = 0.15$  w.r.t. the number of adaptive refinement level

Primal-dual Newton interior point methods for solving the structural optimization problem with a suitable steeplength selection and various strategies for convergence monitoring are discussed in [9]. In the case of elastic

behavior of the composite material numerous computational results are given in [8] for a 2-dimensional specimen and in [10] for a 3-dimensional material workpiece. Computations for an elasto-plastic material body are under considerations and will be presented in a forthcoming paper.

## Acknowledgments

This work has been partially supported by the German National Science Foundation (DFG) under Grant HO877/5-3. The second author has also been supported in part by the Bulgarian Ministry for Education and Science under Grant I1402/2004.

## References

- [1] Allaire G. Shape optimization by the homogenization method. Springer, New York, 2002.
- [2] Ashby M F. Materials and shape. *Acta Metall.*, 1991, 39:1025-1039.
- [3] Asensio G and Moreno C. Linearization and return mapping algorithms for elastoplasticity models. *Int. J. Numer. Methods Eng.*, 2003, 57:991-1014.
- [4] Blaheta R. Convergence of Newton-type methods in incremental return mapping analysis of elasto-plastic problems. *Comput. Methods Appl. Mech. Engrg.*, 1997, 147:167-185.
- [5] Blaheta R and Kohut R. Solution of large nonlinear systems in elastoplastic incremental analysis. *J. Comput. Appl. Math.*, 1995, 63:255-264.
- [6] Delfour M C and Zolésio J-P. Shapes and geometries. Analysis, differential calculus, and optimization. SIAM, Philadelphia, 2001.
- [7] Gibson L J and Ashby M F. Cellular solids, structure, and properties. Pergamon Press, New York, 1988.
- [8] Hoppe R H W and Petrova S I. Optimal shape design in biomimetics based on homogenization and adaptivity. *Math. Comput. Simul.*, 2004, 65(3):257-272.
- [9] Hoppe R H W and Petrova S I. Primal-dual Newton interior point methods in shape and topology optimization. *Numer. Linear Algebra Appl.*, 2004, 11(5-6):413-429.
- [10] Hoppe R H W and Petrova S I. Efficient solvers for 3-D homogenized elasticity model. PARA'04 Workshop on State-of-the-Art in Sci. Comp., June 20-23, 2004, Copenhagen, Denmark. In: *Lect. Notes Comput. Sci.*, Springer (in press).
- [11] Jikov V V, Kozlov S M, and Oleinik O A. Homogenization of differential operators and integral functionals. Springer, 1994.
- [12] Ota T, Takahashi M, Hibi T, Ozawa M, Suzuki S, Hikichi Y, and Suzuki H. Biomimetic process for producing SiC wood. *J. Amer. Ceram. Soc.*, 1995, 78:3409-3411.
- [13] Rozvany G I N. Structural design via optimality criteria. The Prager approach to structural optimization. Dordrecht, Kluwer, 1989.
- [14] Simo J C and Hughes T J R. Computational inelasticity. Springer, 1998.
- [15] Simo J C and Ortiz M. A unified approach to finite deformation elastoplastic analysis based on the use of hyperelastic constitutive equations. *Comput. Methods Appl. Mech. Engrg.*, 1985, 49:221-245.
- [16] Simo J C and Taylor R L. Consistent tangent operators for rate-independent elastoplasticity. *Comput. Methods Appl. Mech. Engrg.*, 1985, 48:101-118.
- [17] Zhang Z L. Explicit consistent tangent moduli with a return mapping algorithm for pressure-dependent elastoplasticity models. *Comput. Methods Appl. Mech. Engrg.*, 1995, 121:29-44.